scientific reports

Check for updates

OPEN

Jorunnamycin A induces apoptosis in pancreatic ductal adenocarcinoma cells, spheroids, and patient-derived organoids by modulating KRAS-mediated survival pathways

Hnin Ei Ei Khine[1], Utid Suriya[2], Thanyada Rungrotmongkol[3,4], Supakarn Chamni[5,6], Yanxi Lu[7], Alan Bénard[7], Bin Lan[7,8], Debabrata Mukhopadhyay[9], David Chang[10], Andrew Biankin[11], Regine Schneider-Stock[11], Robert Grützmann[7], Rungroch Sungthong[1], Christian Pilarsky[7]✉ & Chatchai Chaotham[1]✉

Pancreatic ductal adenocarcinoma (PDAC) is an aggressive malignancy with a poor prognosis, frequently driven by oncogenic *KRAS* mutations. Among these, *KRAS* G12D is the most prevalent, contributing to chemoresistance and limiting the efficacy of current therapeutic strategies. This study investigates the therapeutic potential of jorunnamycin A (JA), a bioactive compound derived from the marine sponge *Xestospongia*, in PDAC. Molecular docking analyses were performed to assess JA's binding affinity for various KRAS protein variants. The synergistic effects of JA in combination with standard chemotherapeutic agents were evaluated using the Bliss independence model in pancreatic cancer cell lines and patient-derived PDAC organoids harboring distinct *KRAS* mutations. Furthermore, western blot analysis was performed to examine the impact the molecular mechanisms underlying JA's anticancer activity. JA demonstrated potent anticancer activity against PDAC cells, irrespective of their *KRAS* mutation status. In silico molecular docking and protein suppression studies indicated a strong binding affinity between JA and KRAS G12D. Synergistic interactions between JA and various PDAC chemotherapeutic agents, including oxaliplatin, SN-38, paclitaxel, 5-fluorouracil, and gemcitabine, were observed using the Bliss independence model. Notably, co-treatment with JA at a 10-fold lower concentration significantly enhanced the cytotoxicity of oxaliplatin, reducing its IC_{50} values around tenfold. This synergistic impact was further validated in both *KRAS* G12D spheroids and patient-derived PDAC organoids harboring *KRAS* G12D and other *KRAS* variants. Mechanistically, the JA-oxaliplatin combination enhanced caspase-3/7 activation, suppressed key *KRAS*-mediated survival pathways (STAT3, B/C-RAF, AKT, and ERK), and led to the downregulation of anti-apoptotic proteins (MCL-1 and BCL-2). These findings highlight JA as a promising therapeutic candidate for PDAC, particularly in the context of *KRAS* G12D-driven tumors. Further investigations into its pharmacokinetics and clinical feasibility are warranted to explore its full potential in PDAC treatment.

Keywords Jorunnamycin A, Pancreatic ductal adenocarcinoma, *KRAS* mutation, *KRAS* G12D, Chemotherapy, Chemosensitizer, Patient-derived organoids

Abbreviations

AKT	Protein kinase B
BCL-2	B-cell lymphoma 2
DMSO	Dimethyl sulfoxide
ERK	Extracellular signal-regulated kinase
FBS	Fetal bovine serum
GDP	Guanosine diphosphate
HRP	Horseradish peroxidase

HS	Horse serum
IC_{50}	Half-maximal inhibitory concentration
JA	Jorunnamycin A
MCL-1	Myeloid cell leukemia 1
MEK	Mitogen-activated protein kinase kinase
PBS	Phosphate-buffered saline
PDAC	Pancreatic ductal adenocarcinoma
PDOs	Patient-derived organoids
PI3K	Phosphatidylinositol 3-kinase
RMSD	Root-mean-square deviation
SDs	Standard deviations
STAT3	Signal transducer and activator of transcription 3
WT	Wild type

[1]Department of Biochemistry and Microbiology, Faculty of Pharmaceutical Sciences, Chulalongkorn University, Bangkok 10330, Thailand. [2]Department of Biochemistry, Faculty of Science, Mahidol University, Bangkok 10400, Thailand. [3]Center of Excellence in Structural and Computational Biology, Department of Biochemistry, Faculty of Science, Chulalongkorn University, Bangkok 10330, Thailand. [4]Program in Bioinformatics and Computational Biology, Graduate School, Chulalongkorn University, Bangkok 10330, Thailand. [5]Department of Pharmacognosy and Pharmaceutical Botany, Faculty of Pharmaceutical Sciences, Chulalongkorn University, Bangkok 10330, Thailand. [6]Natural Products and Nanoparticles Research Unit (NP2), Chulalongkorn University, Bangkok 10330, Thailand. [7]Department of Surgery, Universitätsklinikum Erlangen, Friedrich-Alexander-Universität Erlangen-Nürnberg (FAU), 91054 Erlangen, Germany. [8]Department of Interventional Radiology and Vascular Surgery, Hunan Provincial People's Hospital (The First Affiliated Hospital of Hunan Normal University), Changsha 410002, China. [9]Department of Biochemistry and Molecular Biology, Mayo Clinic College of Medicine and Science, Jacksonville, FL 32224, USA. [10]Wohl Cancer Research Centre, Institute of Cancer Sciences, University of Glasgow, Glasgow G12 8QQ, UK. [11]Experimental Tumor Pathology, Institute of Pathology, Universitätsklinikum Erlangen, Friedrich-Alexander-Universität Erlangen-Nürnberg (FAU), 91054 Erlangen, Germany. ✉email: christian.pilarsky@uk-erlangen.de; chatchai.c@chula.ac.th

Background

Pancreatic ductal adenocarcinoma (PDAC) remains one of the leading causes of cancer-related mortality, despite decades of intensive research into effective treatments. The metastatic nature of PDAC, coupled with the lack of advanced early diagnostic tools, often precludes surgical intervention, making chemotherapy the predominant treatment option[1]. However, the standard regimens–FOLFIRINOX (a combination of oxaliplatin, irinotecan, and 5-fluorouracil) and Gem/Abraxane® (a combination of gemcitabine and nab-paclitaxel)–have proven ineffective in most PDAC patients due to inherent resistance and high relapse rates[2–5]. This limitation highlights the urgent need for novel therapeutic approaches to treat PDAC.

Over 90% of PDAC cases harbor *KRAS* mutations, which contribute to the aggressive and drug-resistant nature of the disease. Among these mutations, G12D is the most common KRAS mutant subtype (40%), followed by G12V (33%)[6–8]. The rarity of intratumoral *KRAS* heterogeneity in PDAC, along with the absence of *KRAS* heterogeneity between primary tumors and metastatic lymph nodes, supports the notion that oncogenic *KRAS* activation serves as the initiating mutation in PDAC development[9]. Targeting *KRAS* holds significant potential to limit disease progression and enhance the chemosensitivity of PDAC[10,11].

Mutated *KRAS* activates a series of critical downstream pathways, including the upregulation of the RAF/mitogen-activated protein kinase kinase (MEK)/extracellular signal-regulated kinase (ERK) and phosphatidylinositol 3-kinase (PI3K)/protein kinase B (AKT) survival cascades, which promote the survival, proliferation, and resistance to cell death in pancreatic cancer cells[12–14]. As a result of ERK and AKT signaling, signal transducer and activator of transcription 3 (STAT3), an important regulator of cell survival and cancer progression, enhances the expression of anti-apoptotic proteins such as myeloid cell leukemia 1 (MCL-1) and B-cell lymphoma 2 (BCL-2)[14,15]. Therefore, understanding KRAS-related molecular biology and targeting these pathways has led to some promising outcomes in current therapeutic strategies aimed at suppressing *KRAS* mutations in PDAC patients[16].

KRAS mutations, excluding the G > T transversions at codons 12 and 13 that lead to the substitution of glutamine with cysteine, were long considered an undruggable target due to the absence of a suitable structural pocket. However, the development of KRAS G12C inhibitors, such as sotorasib and adagrasib, along with preclinical research on MRTX1133–a recently developed selective KRAS G12D inhibitor–has demonstrated the promising potential of targeting mutated KRAS[17]. Moreover, several studies have shown that inhibitors against mutated KRAS, particularly those derived from natural resources, exhibit tumoricidal effect against pancreatic cancer cells and enhance their sensitivity to chemotherapeutic drugs. These natural inhibitors not only have favorable human safety profiles but also suppress KRAS downstream signaling in combination therapies, highlighting their potential as chemo-adjuvant candidates[18]. It is worth noting that there are currently only a few approved drugs targeting mutated KRAS in cancer[6–8].

Jorunnamycin A (JA) (Fig. 1), a bioactive compound isolated from the Thai blue sponge (*Xestospongia*), has demonstrated significant anticancer potential, including the ability to enhance cell susceptibility to anoikis and suppress cancer stem-like phenotypes by modulating the AKT survival pathway in human lung cancer cells harboring *KRAS* mutations[19,20]. A recent study has provided insights into the safety profile of JA and its derivative, 22-(4'py)-JA, unveiling favorable toxicokinetic properties, including the absence of AMES toxicity,

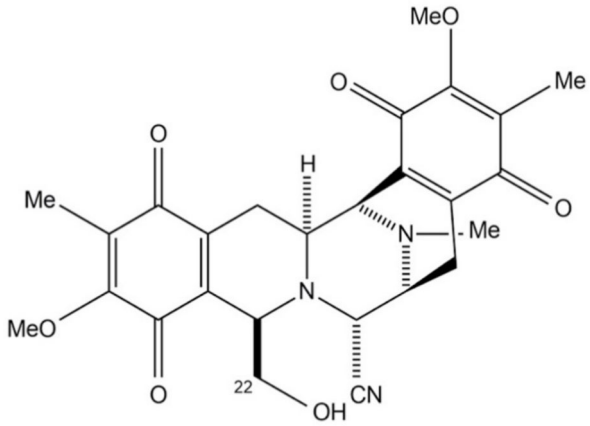

Fig. 1. Chemical structure of jorunnamycin A, isolated from *Xestospongia*.

an acceptable maximum tolerated dose in humans, no skin sensitization, and an oral rat chronic toxicity level of Log 2.25 mg/kg/bw/day[21].

Hitherto, the therapeutic effects of JA, both as a monotherapy and in combination with standard chemotherapeutic agents, on pancreatic cancer cells—particularly in the context of *KRAS* mutations—remain largely unexplored. To better replicate the tumor microenvironment while minimizing reliance on animal models, various three-dimensional cell culture platforms have been established for evaluating the biological activity of emerging therapeutic compounds. Several studies have shown that drug responses in organoid models closely resemble those observed in vivo settings, making them a valuable platform for evaluating potential anticancer agents[22].

In this study, we examined the anticancer potential of JA and its synergistic roles with standard chemotherapeutic agents in various *KRAS*-mutated pancreatic cancer models, including cell lines, spheroids, and patient-derived PDAC organoids. The molecular interactions between JA and different KRAS protein isoforms were analyzed, alongside the underlying mechanisms of its anticancer activity, both as a standalone treatment and in combination with established chemotherapeutics. The derived findings offer valuable insights into JA's therapeutic potential and support its further development as a promising candidate for the treatment of aggressive *KRAS*-mutant PDAC.

Methods

Molecular docking analysis

The structure of KRAS G12D was retrieved from the RCSB Protein Data Bank (PDB ID: 7EWA) and was mutated to G12V, G12C, and WT, using in silico site-directed mutagenesis available in BIOVIA Discovery Studio Visualizer 2021. The structure of JA, used as the ligand, was obtained from PubChem and its geometry was optimized using GaussView 5.0 and Gaussian 16. Local ligand-protein docking was then performed for the four KRAS variants with JA. The binding site was defined using the same coordinates (X: -1.76, Y: -12.41, Z: 11.09) as the co-crystallized compound (KRAS G12D inhibitor, TH-Z827). The box size was set to 10 Å in all dimensions surrounding the crystallized ligand.

Before proceeding with the molecular docking, the protocol was validated by redocking the co-crystallized ligand into the KRAS binding site. The crystallized and redocked conformations were superimposed to assess overlap, represented by the root-mean-square deviation (RMSD) value (Supplementary Information (SI) Fig. S1). A lower RMSD indicates a higher degree of overlap, with an RMSD value of less than 1.0 generally preferred. Subsequently, all docking calculations were performed using the GOLD docking program, with the fitness score employed as the scoring function.

Chemicals, reagents, and biomolecules

JA, with a purity of 95.5% (SI Fig. S2), was extracted from the Thai blue sponge *Xestospongia*, as previously described[19,20]. Oxaliplatin, SN-38, paclitaxel, 5-fluorouracil, and gemcitabine were provided by the pharmacy at University Hospital Erlangen, Germany. The following chemicals were obtained from Sigma-Aldrich (St. Louis, MO, USA): 0.25% trypsin, dimethyl sulfoxide (DMSO), Dulbecco's phosphate-buffered saline (DPBS), phosphate-buffered saline (PBS), skim milk powder, DNase I, *N*-acetylcysteine, nicotinamide, and Y-27,632.

Antibodies specific to G12D Ras (Cat# 14429, RRID: AB_2728748), Ras (Cat# 3339, RRID: AB_2269641), p-AKT (Ser473; Cat# 4060, RRID: AB_2315049), AKT (Cat# 4691, RRID: AB_915783), p-ERK (Thr202/Tyr204; Cat# # 9101, RRID: AB_2315112), ERK (Cat# 9102, RRID: AB_330744), p-B-RAF (Ser445; Cat# 2696, RRID: AB_390721), B-RAF (Cat# 14814, RRID: AB_2750887), p-C-RAF (Ser338; Cat# 9427, RRID: AB_2067317), C-RAF (Cat# 53745, RRID: AB_2799444), p-STAT3 (Tyr705; Cat# 9145, RRID: AB_2491009), STAT3 (Cat# 12640, RRID: AB_2629499), PARP (Cat# 9542, RRID: AB_2160739), MCL-1 (Cat# 94296, RRID: AB_2722740), BCL-2 (Cat# 3498, RRID: AB_1903907), GAPDH (Cat# 5174, RRID: AB_10622025), horseradish peroxidase

(HRP)-coupled anti-rabbit (Cat# 7074, RRID: AB_2099233), and HRP-conjugated anti-mouse (Cat# 7076, RRID: AB_330924) were purchased from Cell Signaling Technology (Danvers, MA, USA).

SuperSignal™ West Pico PLUS Chemiluminescent Substrate, penicillin/streptomycin solution, HEPES, L-glutamine, and B27 supplements were obtained from Thermo Fisher Scientific (Waltham, MA, USA). All experiments utilized ultrapure water produced by the Milli-Q® system from Merck (Darmstadt, Germany).

Cell cultures and formation of cancer spheroids

The human pancreatic cancer cell lines used in this study included SUIT-2 (*KRAS* G12D; JCRB 1094, RRID: CVCL_3172), purchased from the Japanese Collection of Research Bioresources (JCRB) Cell Bank, Tokyo, Japan, along with its CRISPR/Cas9 knockout *KRAS* G12D clones (SUIT-2 1.6, SUIT-2 1.10, SUIT-2 2.4, SUIT-2 2.7, SUIT-2 2.8) generated for this study. The PANC-1 cell line (*KRAS* G12D; ATCC Cat# CRL-1469) was obtained from the American Type Culture Collection (ATCC), Manassas, VA, USA, and its CRISPR/Cas9 knockout *KRAS* G12D clones (PANC-1 2.1, PANC-1 2.2, PANC-1 2.4, PANC-1 2.8, PANC-1 2.9, PANC-1 2.14) were also generated for this study. Additional cell lines included AsPC-1 (*KRAS* G12D; ATCC Cat# CRL-1682), HPAF-II (*KRAS* G12D; ATCC Cat# CRL-1997), HPAC (*KRAS* G12D; ATTC Cat# CRL-2119), SU 86.86 (*KRAS* G12D; ATCC Cat# CRL-1837), Capan-1 (*KRAS* G12V; ATCC Cat# HTB-79), Capan-2 (*KRAS* G12V; ATCC Cat# HTB-80), and MIA PaCa-2 (*KRAS* G12C; ATCC Cat# CRL-1420).

The TKCC-2.1 Lo (*KRAS* G12D), TKCC-10 (*KRAS* G12V), and TKCC-22 Lo (*KRAS* G12V) cell lines were generously provided by David Chang, while the MAYO4636 cell line (*KRAS* G12V) was kindly provided by Debabrata Mukhopadhyay. The PaCaDD-161 cell line (*KRAS* G12V; DSMZ no.: ACC 746) was purchased from the German Collection of Microorganisms and Cell Cultures (DSMZ), Braunschweig, Germany. Additionally, the primary mouse pancreatic cancer TB32047 cell line (*KRAS* G12D) was kindly provided by David Tuveson at Cold Spring Harbor Laboratory (Cold Spring Harbor, NY, USA), while its CRISPR/Cas9 knockout *KRAS* G12D clones (TB32047 1.7, TB32047 1.8, TB32047 1.12, TB32047 1.14, TB32047 1.18) and oxaliplatin-resistant TB32047 OxR cells (derived from continuous oxaliplatin treatment of parental TB32047 cells) were generated and used in this study.

Non-tumorigenic cells with *KRAS* WT included human pancreatic duct epithelial (HPDE E6E7) cells (ATCC Cat# CRL-4039) generously supplied by Ming Tsao from the University of Toronto, Canada, and human embryonic kidney (HEK293 TN) cells obtained from BioCat (Heidelberg, Germany). The presence of *KRAS* mutations (G12D, G12C, and G12V) and CRISPR/Cas9 knockout *KRAS* G12D in all pancreatic cancer cell lines, was previously confirmed in studies[23–26] and validated through Western blot analysis (SI Fig. S3).

Culture media, fetal bovine serum (FBS), and horse serum (HS) were purchased from Thermo Fisher Scientific (Darmstadt, Germany). All cells and organoids[27] were routinely cultured in condition-specific media (SI Table S1) and incubated in a humidified atmosphere with 5% CO_2 at 37 °C. *Mycoplasma* contamination was regularly tested using the Venor® GeM OneStep kit (Minerva Biolabs, Berlin, Germany) to ensure the cultures were *Mycoplasma*-free.

To assess the anticancer activity of JA and its combination with other standard chemotherapeutic agents in different forms of PDAC, cancer spheroids were constructed from the chosen PDAC cell lines. Briefly, PDAC cells were seeded into white, opaque, flat-bottomed 96-well plates with the appropriate culture media at a density of 1,500 cells/well in 9 µL of Matrigel™ (Sigma-Aldrich, St. Louis, MO, USA) to generate spheroids. After incubation at 37 °C for 96 h, the developed spheroids were used for further investigations.

Determination of cell viability and death

CellTiter-Glo® Luminescent Cell Viability Assay was conducted to assess the dose-response of various compounds. Cells were treated with different concentrations of JA (0–10 µM), oxaliplatin (0–100 µM), paclitaxel (0–20 µM), SN-38 (0–1,000 nM), gemcitabine (0–80 nM) and 5-fluorouracil (0–12.8 µM) to determine their cytotoxicity and half-maximal inhibitory concentration (IC_{50}) values. Cells were seeded into white, opaque, flat-bottom 96-well plates at a density of 5×10^3 cells/well and allowed to attach overnight at 37 °C. Following attachment, cells were treated with compounds for 72 h. After treatment, 100 µL of Promega CellTiter-Glo® 2.0 Luminescent Reagent (Madison, WI, USA) was added to each well and incubated at 37 °C for 30 min. Luminescence was then measured using an Infinite® 200 PRO Tecan Microplate Reader (Crailsheim, Germany). Cell viability was calculated as the percentage of relative luminescence between treated and untreated cells. The dose-response curves were generated using the four-parameter Dose-Response model in GraphPad Prism 8.0.2 software (San Diego, CA, USA).

To confirm apoptosis, Caspase-3/7 activity was analyzed. Cells were seeded at a density of 5×10^3 cells/well in white, opaque, flat-bottom 96-well plates and incubated with compounds for 72 h. After treatment, 100 µL of Promega Caspase-Glo® 3/7 Luminescent Reagent (Madison, WI, USA) was added to each well and incubated for 30 min. Luminescence was detected using a microplate reader. Caspase-3/7 activity was expressed as the percentage of relative luminescence between treated and untreated cells. The dose-response curves were also generated using the four-parameter Dose-Response model in GraphPad Prism 8.0.2 software.

Determining the synergistic anticancer activity of JA

The Bliss independence principle was applied to evaluate the synergistic effect of JA in combination with chemotherapeutic drugs using dose-response data. The formula[28] is calculated as follows:

$$S_{Bliss} = y_c - [y_1(x_1) + y_2(x_2) - y_1(x_1) \bullet y_2(x_2)]$$

where $y_1(x_1)$ is the effect of drug 1 alone at concentration x_1, $y_2(x_2)$ is the effect of drug 2 alone at concentration x_2, $y_1(x_1) \cdot y_2(x_2)$ is the predicted effect of the two-drug combination based on their individual effects, and y_c is the actual observed effect of the two-drug combination.

To further investigate the levels of synergy, additivity, and antagonism between the combined compounds, Combenefit software (San Diego, CA, US) was used to perform Bliss analysis on the dose-response data. Synergy scores greater than zero indicate that the combined effect of the two compounds exceeds their additive effect, suggesting synergy. Negative scores suggest an antagonistic effect. A higher synergy score indicates stronger synergistic activity of the drug combination[29].

Construction and characterization of patient-derived organoids

Patient-derived organoids were successfully established from tissue samples of pancreatic cancer patients with identity numbers 65, 122, 124, 128, 197, 208, and 242, following the protocol described by Baker et al.[27]. These derived organoids were characterized based on their histopathological status (malignant or normal tissues) and variation in *KRAS* mutations (SI Table S5 and Fig. S9). To determine the dose-response of various compounds, single cells derived from patient-derived organoids were seeded into white, opaque, flat-bottomed 96-well plates with the appropriate culture media at a density of 1,500 cells/well in 9 µL of Matrigel™ (Sigma-Aldrich, St. Louis, MO, USA) to generate organoids. After incubation at 37 °C for 96 h, the developed organoids were used for further investigations.

Flow cytometry-based apoptosis assay

Apoptosis in patient-derived organoids was evaluated using flow cytometry with annexin V-FITC (Cat# 550474, BD Pharmingen, San Diego, CA, USA) and propidium iodide (PI; Cat# 421301, BioLegend, Amsterdam, Netherlands). Briefly, organoids treated with compounds for 96 h were dissociated into single cells using Trypsin-EDTA. The cells were then washed with PBS (pH 7.4) and stained with annexin V-FITC and PI according to the manufacturer's instructions for 15 min at ambient temperature. The percentage of apoptosis in each sample was assessed using a BD Biosciences LSRII flow cytometer (Heidelberg, Germany).

Western blot analysis

After the indicated treatments, pancreatic cancer cells and PDOs were washed with PBS (pH 7.4) and then incubated on ice with radio-immunoprecipitation assay buffer supplemented with protease inhibitor cocktail (Thermo Fisher Scientific, Waltham, MA, USA) for 45 min to lyse the cell membranes. The cell lysates were then centrifuged at 14,000*g* at 4 °C for 30 min to collect the clear supernatant containing cellular proteins. The total protein content was determined using a BCA Protein Assay kit (Thermo Fisher Scientific, Waltham, MA, USA). Equal amounts of protein (15 µg per sample) were loaded and separated by 10% (w/v) sodium dodecyl sulfate-polyacrylamide gel electrophoresis. The separated proteins were then transferred onto nitrocellulose membranes (Bio-Rad Laboratories, Hercules, CA, USA), which were blocked with 5% skim milk in TBST buffer (Tris buffered saline with 0.1% tween 20, pH 7.2) at room temperature for 2 h.

The membranes were immunoblotted with specific primary antibodies overnight at 4 °C, followed by three washes with TBST buffer for 7 min each. The membranes were then incubated with HRP-linked secondary antibodies at room temperature for 1 h. Finally, the reactive protein signals were detected using SignalFire™ ECL reagent (Cell Signaling Technology, Danvers, MA, USA) and visualized using an Amersham Imager 600 (Pittsburgh, PA, USA). The protein bands were quantified using ImageJ software (Java 1.8.0_172).

Statistical analysis

Numerical data are reported as means ± standard deviations (SDs) from three independent experiments ($n = 3$). Statistical comparisons of means were performed using one-way analysis of variance (ANOVA) with Tukey's post hoc test in GraphPad Prism 8.0.2 software. A p-value < 0.05 was considered statistically significant.

Results

High binding affinity between JA and KRAS G12D

In silico molecular docking analysis was conducted to predict the interactions between JA and wild-type (WT) KRAS, as well as its mutant variants (G12D, G12V, and G12C) (Fig. 2). The docking affinity, evaluated using the fitness score, revealed that JA interacted with all KRAS isoforms tested, albeit with varying binding strengths (Fig. 2A). Ligand-protein interaction analysis indicated that JA bound to WT KRAS at a site near Mg^{2+} and guanosine diphosphate (GDP), resulting in distinct interaction patterns with surrounding residues. Among the KRAS variants, JA exhibited the highest binding affinity for G12D, followed by G12V, KRAS WT, and G12C. Although JA formed interactions with different amino acid residues across the mutant subtypes, the binding patterns involving Glu62, Tyr64, Arg68, His95, and Tyr96 were notably similar between G12D and G12V (Fig. 2B). Hydrogen bonding and hydrophobic interactions were identified as the primary intermolecular forces responsible for JA's binding affinity.

JA as a potent anti-PDAC agent

To determine the half-maximal inhibitory concentration (IC_{50}) and evaluate the selective targeting of different *KRAS* mutations, the cytotoxic profiles of JA were examined in various PDAC cell lines, including those harboring the *KRAS* G12D and other *KRAS* variants. Two non-tumorigenic cell lines with WT *KRAS*, human pancreatic duct epithelial (HPDE E6E7) cells and human embryonic kidney (HEK293 TN) cells, were included in the analysis (Table 1). After 72 h of JA (0–10 µM) treatment, cell viability was significantly reduced in both PDAC and non-tumorigenic cells in a dose-dependent manner (SI Fig. S4). The IC_{50} values for JA in *KRAS*

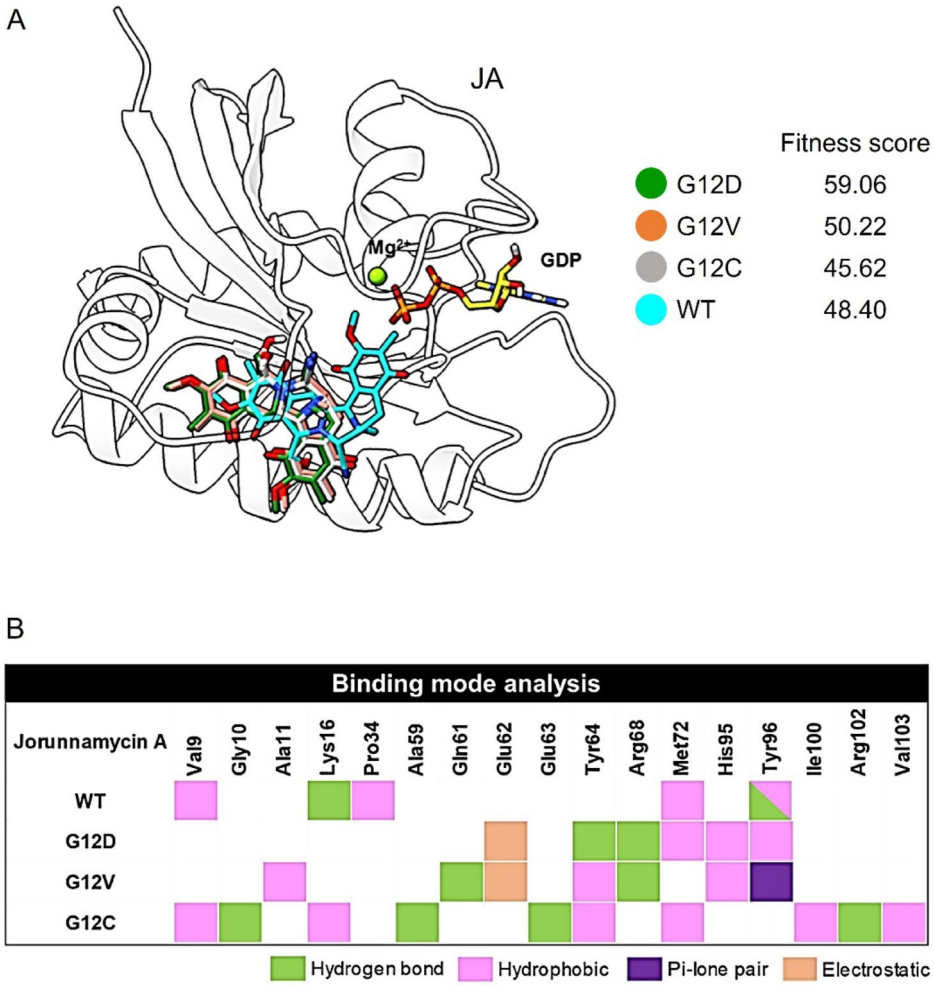

Fig. 2. Docked orientation of jorunnamycin A (JA) with different KRAS variants, along with fitness scores estimated using the GOLD docking program (**A**). Intermolecular interactions between JA and KRAS mutant subtypes (G12D, G12V, or G12C) or wild type (WT) KRAS, are listed (**B**).

G12D variants (0.36–0.86 μM) were approximately 2-fold lower than those observed in *KRAS* G12D knockout clones, cells with other *KRAS* mutations (G12V and G12C), and WT *KRAS* cells (Table 1).

To further investigate the cytotoxic effects of JA in PDAC cells with different *KRAS* variants, the expression levels of apoptosis-related proteins were analyzed (Fig. 3). Treatment with JA (0.5–2 μM) resulted in a dose-dependently increase in cleaved-PARP, a marker of apoptosis, while concurrently reducing the levels of the anti-apoptotic proteins MCL-1 and BCL-2 in *KRAS* G12D cells (Fig. 3A). Similar apoptotic responses were observed in *KRAS* G12D knockout (Fig. 3B), *KRAS* G12V (Fig. 3C), and *KRAS* G12C (Fig. 3D) cells, particularly at the 2 μM JA concentration.

To verify the selective inhibitory effects of JA on *KRAS* G12D, alterations in KRAS signaling-associated proteins were further examined in PDAC cells with different *KRAS* variants (Fig. 4). Treatment with JA (0.5–2 μM) led to a significant reduction in the phosphorylation levels of key *KRAS* downstream signaling proteins, including B/C-RAF, AKT, ERK, and STAT3, across all tested PDAC cells. The decrease was more pronounced in *KRAS* G12D cells (Fig. 4A) compared to *KRAS* G12D knockout (Fig. 4B), *KRAS* G12V (Fig. 4C), and *KRAS* G12C (Fig. 4D) cells.

JA enhances the efficacy of chemotherapeutic drugs in PDAC cells with KRAS G12D

Nine PDAC cell lines with the *KRAS* G12D mutation were used to evaluate the synergistic anticancer effects of JA and other standard chemotherapeutic agents, including oxaliplatin, SN-38 (an active metabolite of irinotecan), paclitaxel, gemcitabine, and 5-fluorouracil. A luminescent viability assay demonstrated that oxaliplatin (0–100 μM) and SN-38 (0–1000 nM), both alone and in combination with JA, significantly reduced the viability of *KRAS* G12D cells in a dose-dependent manner after treatment for 72 h (SI Figs. S4A and S5).

The IC_{50} values of oxaliplatin ranged from 4.37 to 8.11 μM in *KRAS* G12D cells, except in the oxaliplatin-resistant TB32047 cells (12.32 μM) (Table 2) and in *KRAS* G12D knockout cells (12.34–19.64 μM; SI Table S2). However, the IC_{50} values of SN-38 in *KRAS* G12D knockout cells (7.00–12.47 nM; SI Table S2) were much lower than in *KRAS* G12D cells (39.39–154.30 nM; Table 2), indicating *KRAS* G12D-mediated resistance to SN-38 in

cell	KRAS variant	IC_{50} [μM]
human		
SUIT-2	G12D	0.36
• SUIT-2 1.6	G12D knockout	2.28
• SUIT-2 2.8	G12D knockout	3.24
• SUIT-2 1.10	G12D knockout	1.86
• SUIT-2 2.4	G12D knockout	1.53
• SUIT-2 2.7	G12D knockout	1.55
PANC-1	G12D	0.86
• PANC-1 2.8	G12D knockout	2.61
• PANC-1 2.1	G12D knockout	1.60
• PANC-1 2.2	G12D knockout	6.87
• PANC-1 2.4	G12D knockout	2.67
• PANC-1 2.9	G12D knockout	1.96
• PANC-1 2.14	G12D knockout	1.53
TKCC-2.1 Lo	G12D	0.39
AsPC-1	G12D	0.80
HPAF-II	G12D	0.53
HPAC	G12D	0.42
SU 86.86	G12D	0.72
TKCC-10	G12V	1.64
TKCC-22 Lo	G12V	1.76
MAYO4636	G12V	1.19
Capan-1	G12V	3.40
Capan-2	G12V	18.01
PaCaDD-161	G12V	1.97
MIA PaCa-2	G12C	6.72
HEK293 TN	WT	1.90
HDPE E6F7	WT	1.38
mouse		
TB32047	G12D	0.37
• TB32047 1.8	G12D knockout	3.74
• TB32047 1.7	G12D knockout	1.30
• TB32047 1.12	G12D knockout	2.20
• TB32047 1.14	G12D knockout	7.73
• TB32047 1.18	G12D knockout	1.49
TB32047 OxR	G12D	0.60

Table 1. Cytotoxic effects of Jorunnamycin A on cells with different *KRAS* variants.[a]. [a] The half-maximal inhibitory concentration (IC_{50}) values of jorunnamycin A (JA) in pancreatic cancer cells with various *KRAS* mutations and in non-tumorigenic wild-type (WT) *KRAS* cells were determined using the four-parameter Dose-Response model. Data represent the mean values from three independent experiments.

PDAC cells. The Bliss independence principle and dose-response data (Fig. 5) showed that JA and oxaliplatin (Fig. 5A) or SN-38 (Fig. 5B) synergistically enhanced the toxicity in *KRAS* G12D cells, particularly when 0.1 μM JA was combined with 2.5 μM oxaliplatin or 20 nM SN-38.

Similarly, a significant dose-dependent reduction in cell viability was observed in *KRAS* G12D cells after treatment with 0–20 μM paclitaxel (SI Fig. S6), 0–12.8 μM 5-fluorouracil (SI Fig. S7), 0–80 nM gemcitabine (SI Fig. S8), and their combinations with JA (0–10 μM) for 72 h (SI Figs. S6–S8). When considering the IC_{50} values of these chemotherapeutic agents (Table 2 and SI Table S2), there was no noticeable difference, suggesting that the *KRAS* G12D mutation did not significantly influence their cytotoxicity in PDAC cells. Although the synergistic effects were observed in AsPC-1 and HPAC cells, JA-paclitaxel treatment resulted in an additive effect in most tested *KRAS* G12D cells (Fig. 5C). The additive effects were also observed with the combination of JA and 5-fluorouracil (Fig. 5D) or gemcitabine (Fig. 5E).

JA and oxaliplatin synergistically induce cancer cell death

To elucidate the mechanisms underlying the synergistic effects of JA and oxaliplatin in *KRAS* G12D cells, we analyzed the impact of this co-treatment on the viability of human SUIT-2 and mouse TB32047 PDAC cells (Fig. 6). These cells were cultured with JA (0–10 μM), oxaliplatin (0–100 μM), or their combinations for 72 h. The

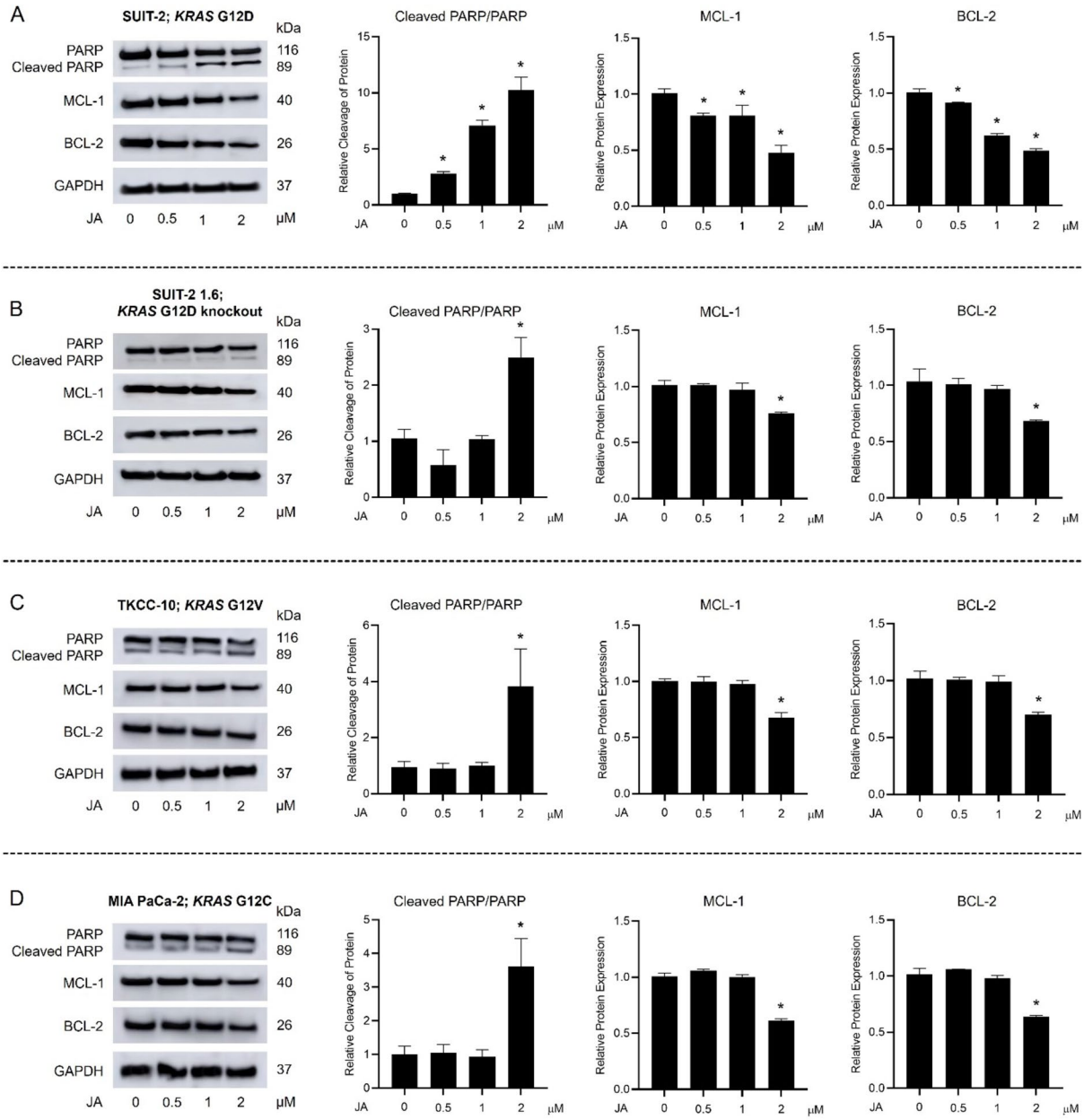

Fig. 3. Jorunnamycin A (JA) and oxaliplatin (Oxa) synergistically enhance pancreatic cancer cell death by modulating apoptosis and survival signals. Human (SUIT-2 (A)) and murine (TB32047 (B)) pancreatic cancer cells harboring *KRAS* G12D, were treated with JA and/or Oxa for 72 h. The effects of the tested compounds and their combination on the expression of apoptosis markers (cleaved PARP/PARP) and the activation of survival signals (MCL-1, BCL-2, STAT3, B/C-RAF, AKT, and ERK) were analyzed by western blotting, with GAPDH as a loading control (see also Supplementary Information Fig. S13 for the original protein bands). The phosphorylated status is denoted as p-. Data are presented as means ± standard deviations from three independent experiments, with asterisks denoting statistically significant differences compared to untreated cells ($p < 0.05$).

Bliss analysis highlighted significant synergistic effects at specific concentrations (Fig. 6A), with a higher level of synergy observed in human PDAC cells compared to murine ones.

Apoptosis analysis revealed increased activity of caspases 3 and 7 in both *KRAS* G12D cell lines after 72 h of co-treatment with JA and oxaliplatin (Fig. 6B). The analysis also demonstrated that the half-maximal effective concentration (EC_{50}) of JA in *KRAS* G12D cells (SUIT-2: 0.45 μM; TB32047: 0.75 μM; Fig. 6C) was more than twice as low as in *KRAS* G12D knockout cells (SUIT-2 1.6: 3.11 μM; TB32047 1.8: 1.98 μM; SI Table S3). Furthermore, the combination of JA and oxaliplatin, particularly at 0.1 μM JA and 2.5 μM oxaliplatin, exhibited significant synergistic apoptotic effects, as demonstrated by the Bliss independence principle (Fig. 6D) and dose-response data from the caspase-3/7 assays in *KRAS* G12D cells.

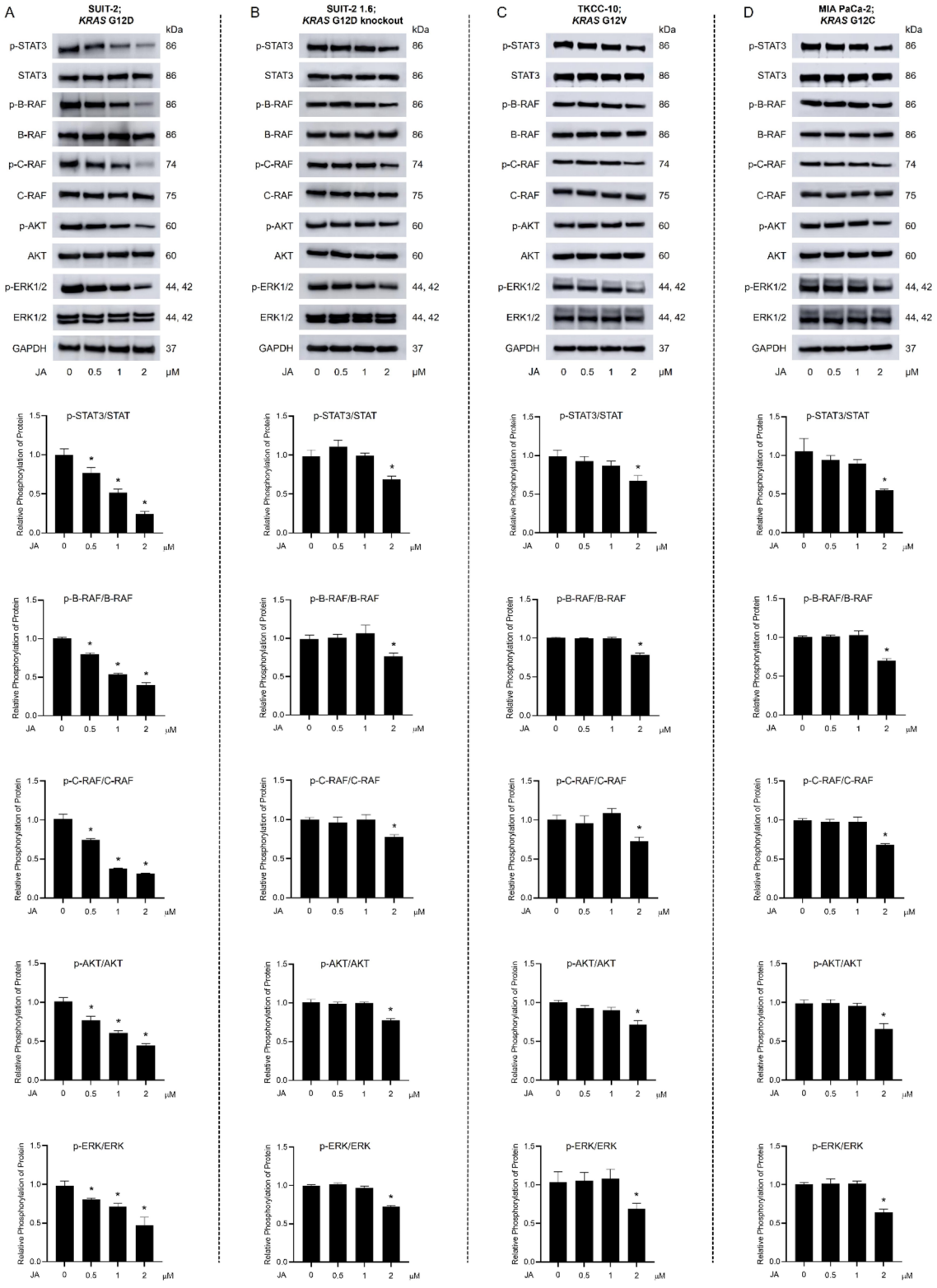

Fig. 4. Jorunnamycin A (JA) induces apoptosis in pancreatic cancer cells. Human pancreatic cancer cells with different *KRAS* variants—SUIT-2; *KRAS* G12D (**A**), SUIT-2 1.6; *KRAS* G12D knockout (**B**), TKCC-10; *KRAS* G12V (**C**), and MIA PaCa-2; *KRAS* G12C (**D**)—were treated with varying concentrations of JA for 72 h. JA's effects on poly (ADP-ribose) polymerase (PARP) cleavage, an apoptosis marker, and the expression of anti-apoptotic proteins (MCL-1 and BCL-2) were assessed using western blot analysis, with GAPDH as a loading control (see also Supplementary Information Fig. S11 for the original protein bands). Data are shown as means ± standard deviations from three independent experiments, with asterisks indicating statistically significant differences compared to untreated cells ($p < 0.05$).

cell	IC_{50}				
	Oxa [μM]	SN-38 [nM]	PTX [μM]	5-FU [μM]	GEM [nM]
human					
SUIT-2	6.45	58.20	9.95	1.72	5.53
PANC-1	8.11	120.90	6.84	1.53	5.28
TKCC-2.1 Lo	4.83	108.90	21.82	1.59	5.39
AsPC-1	5.52	114.50	77.85	0.82	5.54
HPAF-II	4.37	74.20	5.73	0.90	6.37
HPAC	7.28	39.39	10.89	0.89	6.41
SU 86.86	5.77	154.30	68.09	0.79	8.41
mouse					
TB32047	6.10	49.85	9.57	0.52	10.70
TB32047 OxR	12.32	72.63	7.81	0.54	5.58

Table 2. Cytotoxic effects of chemotherapeutic agents on *KRAS* G12D-mutated pancreatic cancer cells.[a]. [a] The half-maximal inhibitory concentration (IC_{50}) values of oxaliplatin (Oxa), SN-38, paclitaxel (PTX), 5-fluorouracil (5-FU), and gemcitabine (GEM) in pancreatic cancer cells harboring *KRAS* G12D were determined using the four-parameter Dose-Response model. Data represent the mean values from three independent experiments.

JA and oxaliplatin synergistically downregulate KRAS -mediated signals

To elucidate the mechanism behind the synergistic effect (Fig. 7), non-toxic concentrations of JA were selected to ensure that any observed cellular activities were specifically due to the interaction between this compound and oxaliplatin rather than toxicity from high concentrations. Optimal non-toxic concentrations of 0.1 μM JA and 2.5 μM oxaliplatin were chosen for investigation in *KRAS* G12D PDAC cells. In both human SUIT-2 (Fig. 7A) and murine TB32047 (Fig. 7B) *KRAS* G12D cells, treatment with either JA or oxaliplatin alone did not alter the expression of cleaved PARP/PARP, MCL-1, and BCL-2. Notably, JA-oxaliplatin co-treatment for 72 h significantly decreased the expression of MCL-1 and BCL-2 and dramatically increased the level of cleaved PARP/PARP, in both *KRAS* G12D PDAC cells. The combination of JA and oxaliplatin significantly deactivated other *KRAS* downstream signaling proteins (B/C-RAF, AKT, ERK, and STAT3) in both SUIT-2 (Fig. 7A) and TB32047 (Fig. 7B) cells, which were not observed in the individual treatments.

In addition to the in vitro monolayer cell culture assays, cancer spheroids generated from SUIT-2 and TB32047 cells were employed to confirm the synergistic effects of JA-oxaliplatin co-treatment (Fig. 8). Treatments for 96 h with either compound alone or in combination remarkably reduced viability in all constructed PDAC spheroids (Fig. 8A). The IC_{50} value of JA was approximately 3-fold higher in PDAC spheroids derived from *KRAS* G12D knockout cells (SUIT-2 1.6: 2.32 μM; TB32047 1.8: 3.33 μM; SI Table S4) compared to those derived from *KRAS* G12D cells (SUIT-2: 0.73 μM; TB32047: 0.87 μM; Fig. 8B), confirming the *KRAS* G12D-dependent anticancer activity of JA. With the Bliss independence principle, the JA-oxaliplatin co-treatment exhibited a substantial synergistic effect in all constructed PDAC spheroids, particularly at 1 μM JA and 10 μM oxaliplatin (Fig. 8C).

PDAC patient-derived organoids confirm JA-oxaliplatin synergistic anticancer activity

Organoids derived from PDAC patients' tissues were employed to evaluate the synergistic effects of co-treatment with JA and oxaliplatin (Fig. 9). PDAC organoids with different *KRAS* variants were identified and generated from 8 patients (SI Table S5 and Fig. S9), including *KRAS* G12D (Panc124, Panc128, and Panc197 T2 organoids), *KRAS* G12V (Panc122 and Panc208 organoids), *KRAS* G12S (Panc65 organoid), *KRAS* G12R (Panc197 T1 organoid), WT *KRAS* (Panc242 N). The Panc242 N organoid harboring WT *KRAS* was characterized as a non-malignant organoid derived from normal pancreatic ductal tissues and confirmed by a histopathological assessment.

Viability of all tested organoids was assessed after treating with JA, oxaliplatin, or their combination for 96 h (Fig. 9A-H). JA exhibited higher toxicity in *KRAS* G12D organoids, with IC_{50} values ranging from 0.62 to 0.86 μM (Fig. 9I), compared to organoids with other oncogenic *KRAS* variants (G12V, G12R, and G12S) and non-malignant WT *KRAS* (Panc242 N). Interestingly, oxaliplatin did not show significant difference in IC_{50} values across all tested organoids. Furthermore, combination treatment with 1 μM JA and 10 μM oxaliplatin demonstrated a synergistic effect in all cancer organoids (Fig. 9J).

Given the high prevalence of the *KRAS* G12D and G12V mutations in PDAC[6,8], the expression of apoptosis-related proteins was examined in Panc124 (*KRAS* G12D) and Panc122 (*KRAS* G12V) organoids to explore molecular mechanisms underlying the anticancer activity of JA-oxaliplatin co-treatment (Fig. 10). A marked increase in cleavage PARP/PARP levels and a decreased in MCL-1 and BCL-2 protein expression were observed in both organoids treated with 1–2 μM JA for 96 h, as shown in Fig. 10A and C. Notably, JA exhibited potent anticancer activity against *KRAS* G12D organoids at a low concentration of 0.5 μM, as evidenced by significant alterations in apoptosis-related proteins (Fig. 10A).

To further assess their synergistic effects, Panc122 and Panc124 organoids were co-treated with noncytotoxic concentrations of JA and oxaliplatin (Fig. 10B, D). The combination of JA (0.1 μM) and oxaliplatin (2.5 μM) not only reduced MCL-1 and BCL-2 expression but also elevated cleaved PARP/PARP levels in both Panc124

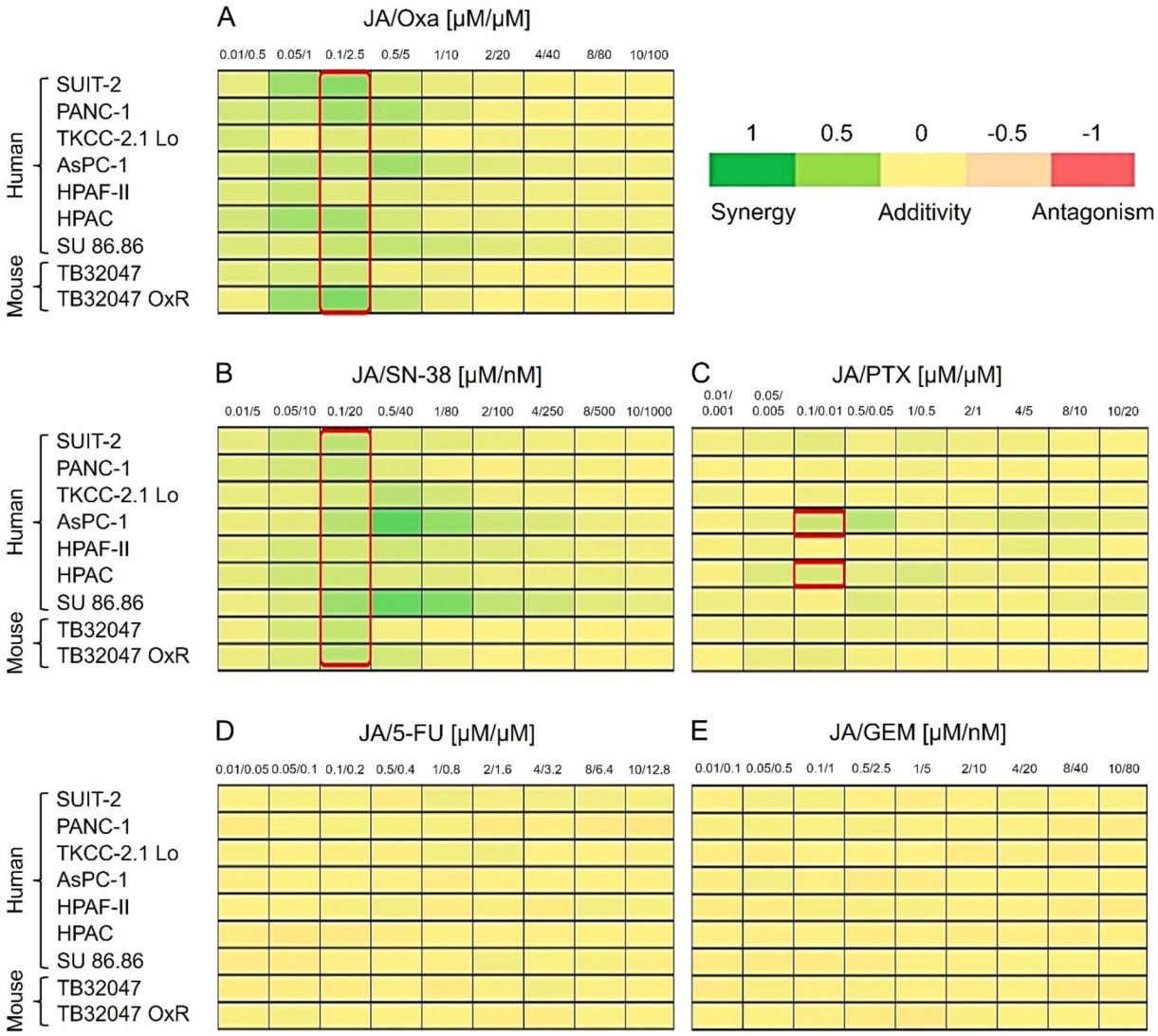

Fig. 5. Synergistic anticancer effects of jorunnamycin A (JA) and standard chemotherapeutic drugs in pancreatic cancer cells. Human (SUIT-2, PANC-1, TKCC-2.1 Lo, AsPC-1, HPAF-II, HPAC, and SU 86.86) and murine (TB32047 and TB32047 OxR) pancreatic cancer cells harboring *KRAS* G12D, were treated for 72 h with varying concentrations of JA and different chemotherapeutic agents: oxaliplatin (Oxa) (**A**), SN-38 (**B**), paclitaxel (PTX) (**C**), 5-fluorouracil (5-FU) (**D**), and gemcitabine (GEM) (**E**). Synergistic effects identified using the Bliss independence principle are highlighted in red boxes, and interaction scores are represented as color scales. All experiments were performed in triplicate.

(Fig. 10B) and Panc122 (Fig. 10D) organoids. Remarkably, these dramatic alterations in apoptosis proteins were most pronounced in the *KRAS* G12D Panc124 organoids.

Shrinkage morphology (SI Fig. S10) and flow cytometry histograms (Fig. 10E) revealed increased apoptosis in *KRAS* G12D Panc124 and *KRAS* G12V Panc122 organoids co-treated with noncytotoxic concentrations of JA and oxaliplatin. Although no significant apoptosis was observed with individual treatment, co-treatment clearly triggered apoptosis in both organoids. Significantly higher percentages of apoptosis were observed in Panc124 compared to Panc122 organoids (Fig. 10F).

Discussion

Natural compounds have long been recognized for their therapeutic potential and safety, making them become valuable sources for the development of novel pharmacotherapies. In the field of oncology, emerging chemotherapeutic agents, such as ecteinascidin 743 and halichondrin B (currently in phase 2 clinical trials), have been successfully developed from natural sources[30]. Recently, JA, a marine alkaloid isolated from the sponge *Xestospongia*, has demonstrated potential in inhibiting metastasis and suppressing the cancer stem-like phenotypes in human lung cancer cells[19–21]. In this study, we further extended JA's pharmacotherapeutic potential in defeating PDAC, employing a variety of PDAC models (cell cultures, spheroids, and patient-derived organoids) harboring various *KRAS* variants.

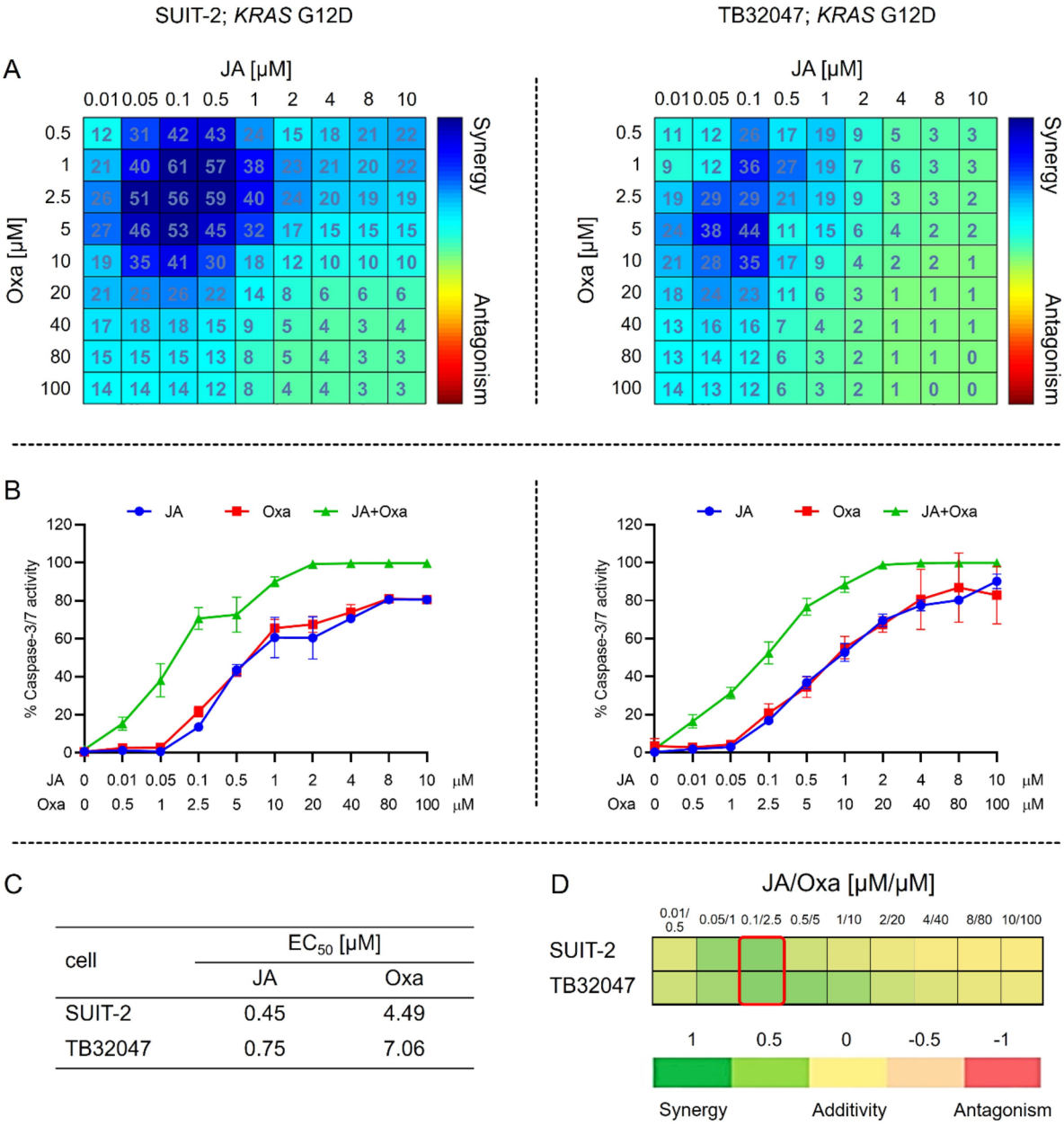

cell	EC_{50} [μM]	
	JA	Oxa
SUIT-2	0.45	4.49
TB32047	0.75	7.06

Fig. 6. Jorunnamycin A (JA) and oxaliplatin (Oxa) synergistically enhance pancreatic cancer cell death by upregulating caspase-3/7. Human (SUIT-2) and murine (TB32047) pancreatic cancer cells harboring *KRAS* G12D, were treated for 72 h with varying concentrations of JA and/or Oxa. The synergistic effect of the tested compounds and their combination on cell viability was assessed using Combenefit software and visualized with color scales (**A**). Caspase-3/7 mediated apoptosis was evaluated using the caspase-3/7 activity assay (**B**), with half-maximal effective concentrations (EC_{50}) calculated (**C**). Synergistic interactions, identified via the Bliss independence principle, are highlighted in a red box, while interaction scores shown as color scales (**D**). All experiments were conducted in triplicate.

Among the various single mutations in *KRAS* gene observed in different tumor types, approximately 40% of *KRAS* mutations in PDAC involve a single-base missense mutation at G12D[7,8]. KRAS G12D is known for its low GTPase activity during both intrinsic and GAP-activated stages, leading to sustained activation of KRAS[31]. Despite the higher IC_{50} values, the similar amino acid interaction patterns between KRAS G12D and G12V suggest that JA may benefit the treatment of PDAC harboring *KRAS* G12V variant, the second most common *KRAS* mutation in cancer patients[32]. The interactions between JA and KRAS at the Glu62 and His95 residues align with those of potent KRAS G12D inhibitors like TH-Z816 and KRAS G12C inhibitors such as adagrasib (MRTX849)[33,34]. Notably, available KRAS G12C inhibitors covalently bind with His95 (e.g., sotorasib and ARS-1620) and Tyr96 (sotorasib), whereas JA does not interact with these residues in KRAS G12C[35]. These interactions may contribute to the increased binding affinity of JA to KRAS G12D and G12V compared to

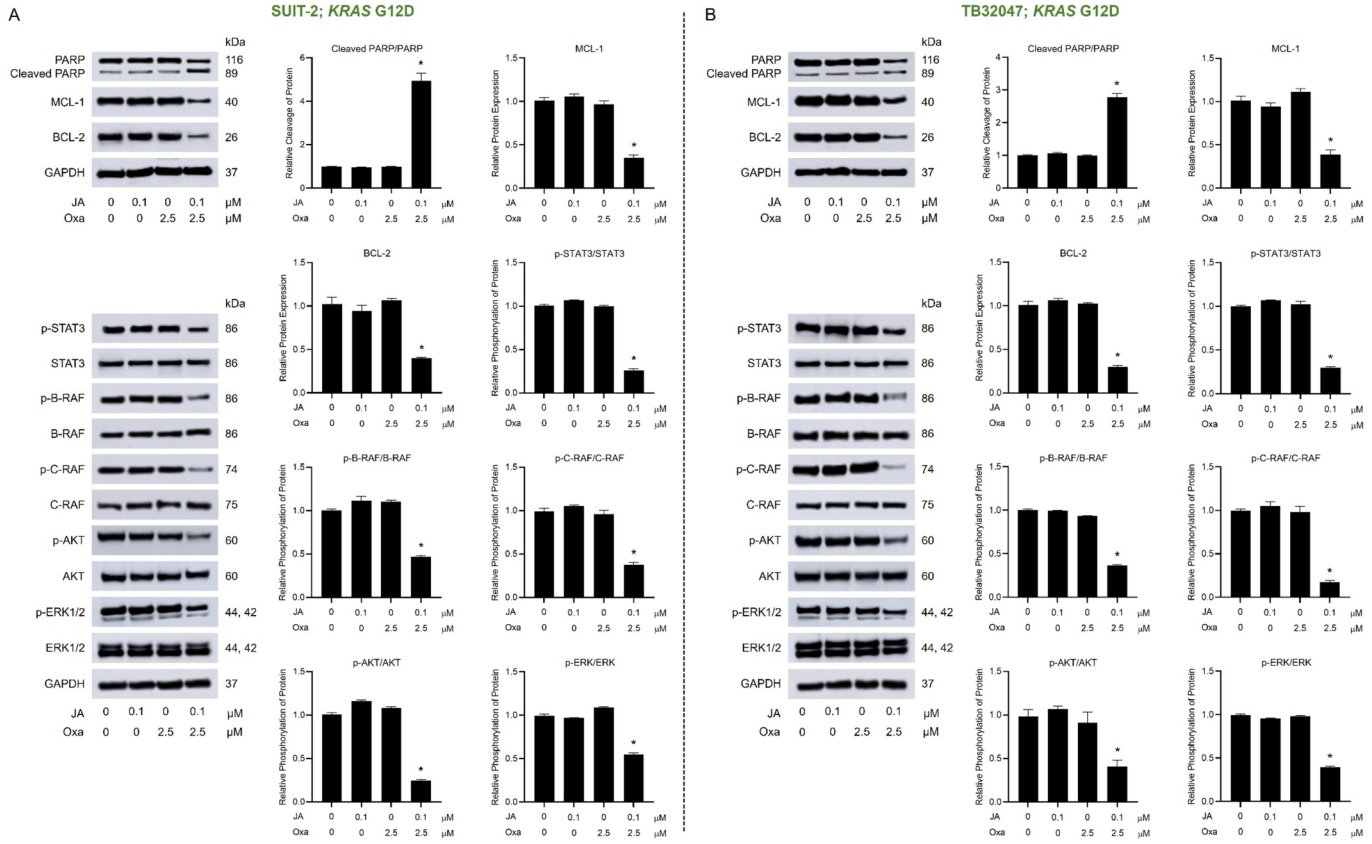

Fig. 7. Jorunnamycin A (JA) and oxaliplatin (Oxa) synergistically enhance pancreatic cancer cell death by modulating apoptosis and survival signals. Human (SUIT-2 (**A**)) and murine (TB32047 (**B**)) pancreatic cancer cells harboring *KRAS* G12D, were treated with JA and/or Oxa for 72 h. The effects of the tested compounds and their combination on the expression of apoptosis markers (cleaved PARP/PARP) and the activation of survival signals (MCL-1, BCL-2, STAT3, B/C-RAF, AKT, and ERK) were analyzed by western blotting, with GAPDH as a loading control (see also Supplementary Information Fig. S13 for the original protein bands). The phosphorylated status is denoted as p-. Data are presented as means ± standard deviations from three independent experiments, with asterisks denoting statistically significant differences compared to untreated cells ($p < 0.05$).

WT KRAS and KRAS G12C. However, further studies, including molecular dynamics simulations and alanine scanning, are needed to identify the crucial hot-spot amino acids governing JA binding.

KRAS has historically been considered an undruggable target due to its lack of structural pocket and its strong binding affinity to GTP and GDP at picomolar dosages[31,36–38]. However, the discovery of KRAS G12C-specific inhibitors that interact with the switch-II region of KRAS in its inactive state has paved the way for KRAS-targeted therapies with promising clinical outcomes[39]. The amino acids within residues 58–72 of KRAS, which constitute the switch-II region are responsible for binding and activating downstream effector molecules[40]. Recently, the switch-II pocket has been proposed as a novel drug-binding site, especially for mutated *KRAS* oncogenes that do not require covalent interactions[41]. TH-Z816, a KRAS G12D inhibitor that binds at Glu62, Gly60, and Met72, significantly suppresses the RAF/MEK/ERK and PI3K/AKT survival pathways in pancreatic cancer cells[33]. Correspondingly, the downregulation of KRAS-mediated survival signals in *KRAS* G12D pancreatic cancer cells treated with JA may result from JA's binding ability at the switch-II region of KRAS G12D.

Targeted therapies have not only improved survival rates but also minimized side effects compared to standard chemotherapy. However, the benefits of specific KRAS inhibitors may be limited due to the development of acquired drug resistance, like conventional chemotherapy. To counteract chemo-resistance and maximize therapeutic benefits with fewer side effects, combination therapy is proposed as a promising strategy[12]. The synergistic effect of JA was demonstrated in *KRAS* G12D PDAC cells when combined with DNA-modifying anticancer drugs such as oxaliplatin and SN-38. In contrast, co-treatment with JA and paclitaxel or antimetabolites (gemcitabine and 5-fluorouracil) resulted in an additive effect. The varying anticancer effects of different drug combinations in *KRAS* G12D PDAC cells may stem from differences in chemosensitivity[42]. The synergy between JA and oxaliplatin was also observed in PDAC spheroids and patient-derived PDAC organoids. It is worth noting that *KRAS* G12D PDAC cells were more resistant to SN-38 alone, but this resistance was overcome by its combination with JA. The complex structure of cancer organoids generated from patient tissues led to more than double the IC_{50} values of JA compared to those observed in cell culture and spheroid

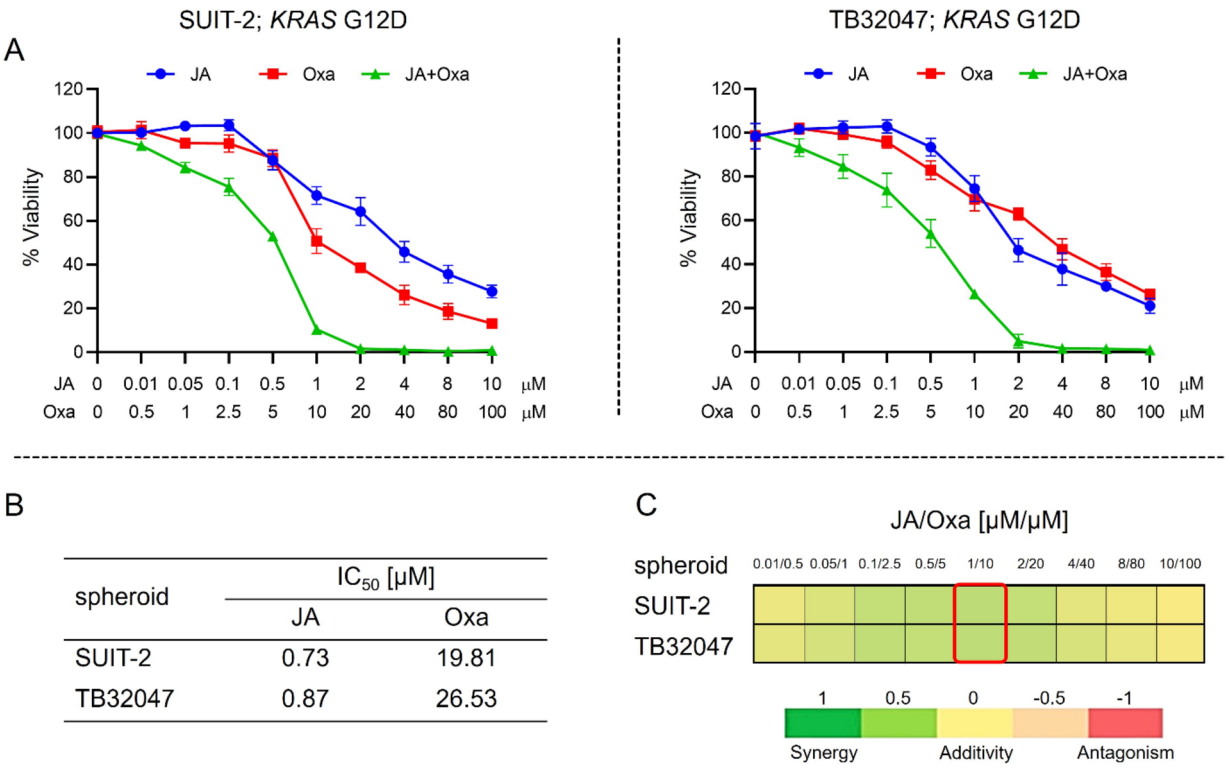

spheroid	IC_{50} [μM]	
	JA	Oxa
SUIT-2	0.73	19.81
TB32047	0.87	26.53

Fig. 8. Jorunnamycin A (JA) and oxaliplatin (Oxa) synergistically enhance apoptosis in pancreatic cancer spheroids. Human (SUIT-2) and murine (TB32047) spheroids harboring *KRAS* G12D, were constructed for 96 h and treated with varying concentrations of JA and/or Oxa for 96 h. The synergistic effect on spheroid viability was evaluated using the CellTiter-Glo® Luminescent Cell Viability Assay (**A**), with half-maximal inhibitory concentration (IC_{50}) values calculated (**B**). Synergistic interactions identified through the Bliss independence principle are highlighted in a red box, and interaction scores are displayed as color scales (**C**). All experiments were performed in triplicate.

assessments, which may have implications for precise pharmacological evaluations prior to clinical trials[43,44]. Our findings have shown that the synergistic interactions between JA and oxaliplatin are highly selective for malignant organoids while minimizing toxicological effects on organoids derived from normal tissues.

Cancer cells harboring *KRAS* G12D mutation express higher levels of ERK and AKT signals compared to *KRAS* G12C-mutant cells[45]. The anticancer activity of JA was confirmed by increased IC_{50} values in isogenic CRISPR/Cas9 knockout *KRAS* G12D PDAC clones. Moreover, the specificity of JA for KRAS G12D was demonstrated by lower IC_{50} values and greater inhibition of KRAS survival signals in *KRAS* G12D-mutant cells compared to the other single-base missense variants, consistent with the binding affinity of JA to KRAS G12D. The downregulation of KRAS downstream signaling proteins (e.g., AKT, RAF, ERK, STAT3, MCL-1, and BCL-2) in *KRAS* G12D PDAC cells co-treated with noncytotoxic concentrations of JA and oxaliplatin provides evidence of a synergistic effect through modulation of KRAS G12D signaling. The combination of JA and oxaliplatin synergistically enhanced chemosensitivity specifically in *KRAS* G12D-mutant cells, spheroids, and patient-derived organoids, but not in *KRAS* WT non-malignant organoids. These findings support the promising clinical application of this combined therapy that may reduce adverse events associated with high-dosing administration of two anticancer drugs[46].

Conclusions

This study highlights the binding affinity and specificity of JA to different KRAS variants, along with its ability to downregulate KRAS-mediated survival signals (AKT, STAT3, RAF, ERK) while simultaneously upregulating apoptotic markers. The synergistic effects of JA in combination with the chemotherapeutic drug, oxaliplatin, observed in PDAC cell cultures, spheroids, and patient-derived organoids, unveil its potent anticancer activity that is promising for further pharmacological assessments and future clinical application. The cytotoxic effects of JA in malignant and normal cells need additional investigation to confirm its safety and efficacy in the development of targeted PDAC therapy. Overall, JA, a natural marine-derived alkaloid, demonstrates significant potential as an anticancer agent for treating aggressive PDAC with *KRAS* G12D mutation, offering a promising strategy to optimize pancreatic cancer pharmacotherapy.

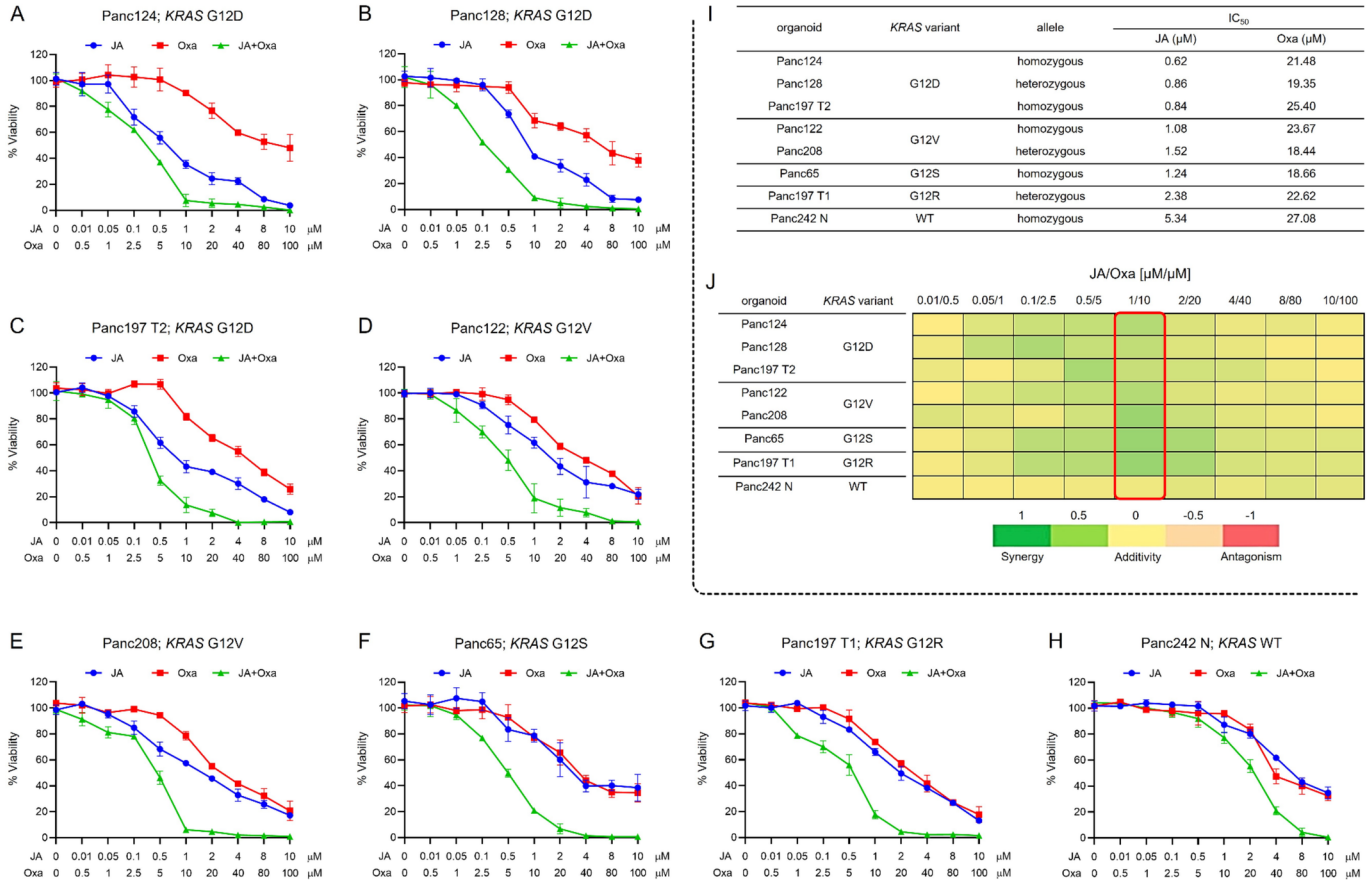

organoid	*KRAS* variant	allele	IC_{50} JA (μM)	IC_{50} Oxa (μM)
Panc124	G12D	homozygous	0.62	21.48
Panc128		heterozygous	0.86	19.35
Panc197 T2		homozygous	0.84	25.40
Panc122	G12V	homozygous	1.08	23.67
Panc208		heterozygous	1.52	18.44
Panc65	G12S	homozygous	1.24	18.66
Panc197 T1	G12R	heterozygous	2.38	22.62
Panc242 N	WT	homozygous	5.34	27.08

Fig. 9. Jorunnamycin A (JA) and oxaliplatin (Oxa) synergistically enhances apoptosis in patient-derived pancreatic cancer organoids. Organoids were developed from patient-derived pancreatic cancer tissues with different *KRAS* variants: Panc124 (**A**), Panc128 (**B**), and Panc197 T2 (**C**) with *KRAS* G12D; Panc122 (**D**) and Panc208 (**E**) with *KRAS* G12V; Panc65 (**F**) with *KRAS* G12S; Panc197 T1 (**G**) with *KRAS* G12R, and Panc242 N (**H**) with wild type (WT) *KRAS*. The Panc242 N organoid served as a non-malignant organoid characterized by histopathological analysis (data not shown). All organoids were treated with varying concentrations of JA and/or Oxa for 96 h. The synergistic effect on organoid viability was evaluated using the CellTiter-Glo Luminescent Cell Viability Assay (A–H), with half-maximal inhibitory concentration (IC_{50}) values calculated (**I**). Synergistic interactions identified through the Bliss independence principle are highlighted in a red box, and interaction scores are displayed as color scales (**J**). All experiments were conducted in triplicate.

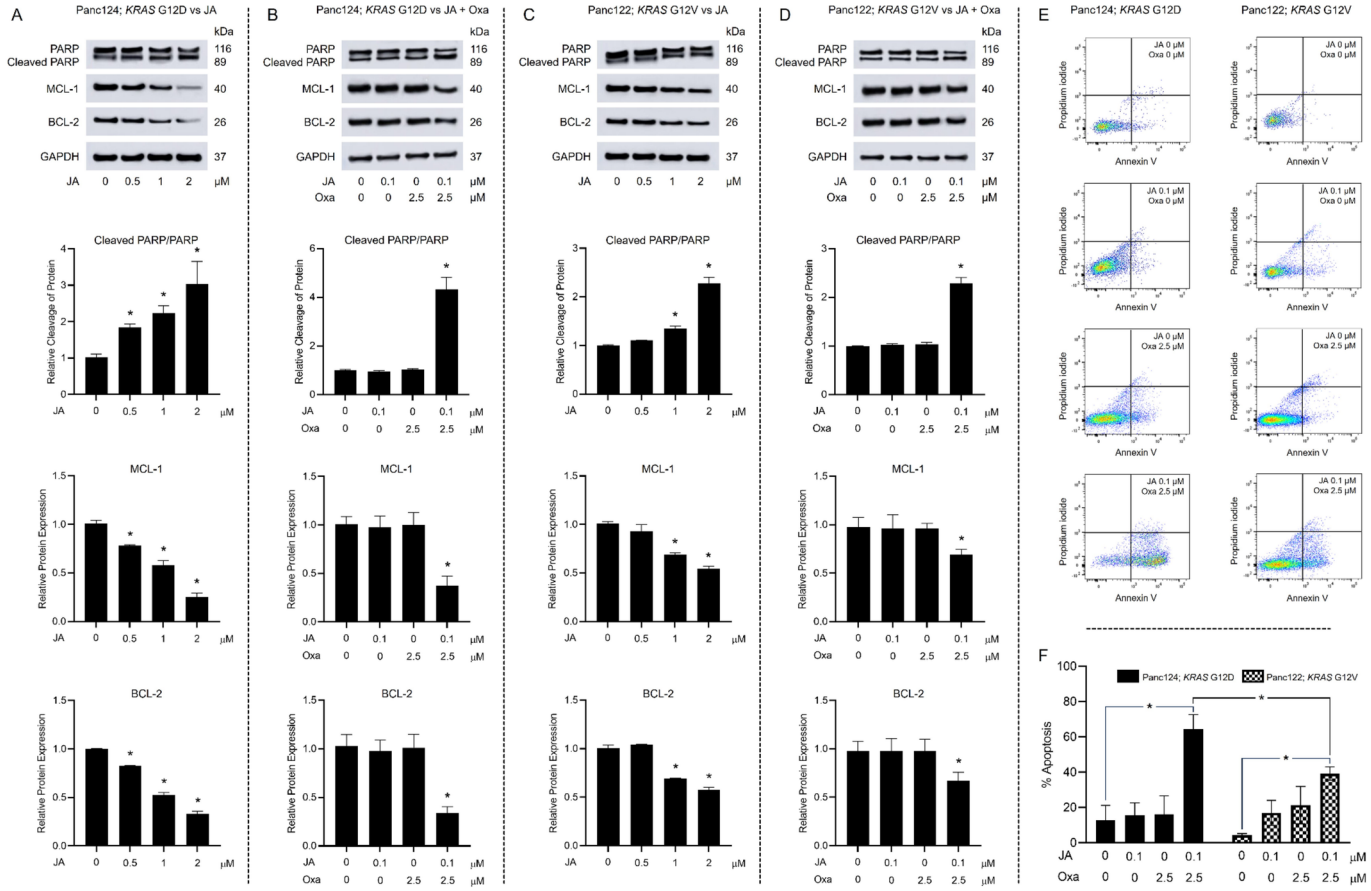

Fig. 10. Jorunnamycin A (JA) and oxaliplatin (Oxa) synergistically enhance apoptosis in patient-derived pancreatic cancer organoids by modulating apoptosis and survival signals. Organoids were developed from patient-derived pancreatic cancer tissues with different *KRAS* variants: Panc124 (A and B) with *KRAS* G12D and Panc122 (C and D) with *KRAS* G12V. Organoids were treated with JA (A, C) or JA and Oxa (B, D) for 96 h. The impacts of JA and Oxa on an apoptosis marker (cleaved PARP/PARP) and survival signals (MCL-1 and BCL-2), were evaluated using western blot analysis, with GAPDH as a loading control (A–D) (see also Supplementary Information Fig. S14 for the original protein bands). Apoptotic organoids exposed to JA and/or Oxa were further quantified via annexin V/propidium iodide-based flow cytometry (E and F). Data are presented as means ± standard deviations from three independent experiments, with asterisks denoting statistically significant differences ($p < 0.05$).

Data availability

All data analyzed during this study are included in this published article and supplementary material.

Received: 10 December 2024; Accepted: 24 March 2025
Published online: 03 April 2025

References

1. Mukhopadhyay, S. et al. Undermining Glutaminolysis bolsters chemotherapy while NRF2 promotes chemoresistance in KRAS-driven pancreatic cancers. *Cancer Res.* **80**, 1630–1643. https://doi.org/10.1158/0008-5472.CAN-19-1363 (2020).
2. Kim, Y. E. et al. SILAC-based quantitative proteomic analysis of oxaliplatin-resistant pancreatic cancer cells. *Cancers* **13**, 724. https://doi.org/10.3390/cancers13040724 (2021).
3. Braun, L. M. et al. Metabolic adaptation during nab-paclitaxel resistance in pancreatic cancer cell lines. *Cells* **9**, 1251. https://doi.org/10.3390/cells9051251 (2020).
4. Skrypek, N. et al. The oncogenic receptor ErbB2 modulates gemcitabine and irinotecan/SN-38 chemoresistance of human pancreatic cancer cells via hCNT1 transporter and multidrug-resistance associated protein MRP-2. *Oncotarget* **613**, 10853–10867. https://doi.org/10.18632/oncotarget.3414 (2015).
5. Wang, W. B. et al. Recent studies of 5-fluorouracil resistance in pancreatic cancer. *World J. Gastroenterol.* **2042**, 15682–15690. https://doi.org/10.3748/wjg.v20.i42.15682 (2014).
6. Yang, K. et al. KRAS promotes tumor metastasis and chemoresistance by repressing RKIP via the MAPK-ERK pathway in pancreatic cancer. *Int. J. Cancer.* **14211**, 2323–2334. https://doi.org/10.1002/ijc.31248 (2018).
7. Bannoura, S. F., Khan, H. Y. & Azmi, A. S. KRAS G12D targeted therapies for pancreatic cancer: has the fortress been conquered? *Front. Oncol.* **12**, 1013902. https://doi.org/10.3389/fonc.2022.1013902 (2022).
8. Shen, H. et al. KRAS G12D mutation subtype in pancreatic ductal adenocarcinoma: does it influence prognosis or stage of disease at presentation? *Cells* **11**, 3175. https://doi.org/10.3390/cells11193175 (2022).

9. Hashimoto, D. et al. Heterogeneity of *KRAS* mutations in pancreatic ductal adenocarcinoma. *Pancreas* **45**, 1111–1114. https://doi.org/10.1097/MPA.0000000000000624 (2016).
10. Tang, D. & Kang, R. Glimmers of hope for targeting oncogenic KRAS-G12D. *Cancer Gene Ther.* **30**, 391–393. https://doi.org/10.1038/s41417-022-00561-3 (2023).
11. Kemp, S. B. et al. Efficacy of a small-molecule inhibitor of $Kras^{G12D}$ in immunocompetent models of pancreatic cancer. *Cancer Discov.* **13**, 298–311. https://doi.org/10.1158/2159-8290.CD-22-1066 (2023).
12. Huang, L. et al. KRAS mutation: from undruggable to druggable in cancer. *Signal. Transduct. Target. Ther.* **6**, 386. https://doi.org/10.1038/s41392-021-00780-4 (2021).
13. Steelman, L. S. et al. Roles of the Raf/MEK/ERK and PI3K/PTEN/Akt/mTOR pathways in controlling growth and sensitivity to therapy-implications for cancer and aging. *Aging* **3**, 192–222. https://doi.org/10.18632/aging.100296 (2011).
14. Mollinedo, F. & Gajate, C. Novel therapeutic approaches for pancreatic cancer by combined targeting of RAF→MEK→ERK signaling and autophagy survival response. *Ann. Transl Med.* **7**, S153. https://doi.org/10.21037/atm.2019 (2019).
15. Wang, H. Q. et al. STAT3 pathway in cancers: Past, present, and future. *MedComm* 3, e135. (2022). https://doi.org/10.1002/mco2.124
16. Khandakar, G. I. et al. ACAGT-007a, an ERK MAPK signaling modulator, in combination with AKT signaling Inhibition induces apoptosis in Kras mutant pancreatic cancer T3M4 and MIA-Pa-Ca-2 cells. *Cells* **11**, 702. https://doi.org/10.3390/cells11040702 (2022).
17. Hashemi, S. et al. Discovery of direct inhibitor of KRAS oncogenic protein by natural products: A combination of pharmacophore search, molecular docking, and molecular dynamic studies. *Res. Pharm. Sci.* **15**, 226–240. https://doi.org/10.4103/1735-5362.288425 (2020).
18. Zhou, X., Ji, Y. & Zhou, J. Multiple strategies to develop small molecular KRAS directly bound inhibitors. *Molecules* **28**, 3615. https://doi.org/10.3390/molecules28083615 (2023).
19. Ecoy, G. A. U. et al. Jorunnamycin A from *Xestospongia* Sp. suppresses epithelial to mesenchymal transition and sensitizes Anoikis in human lung cancer cells. *J. Nat. Prod.* **82**, 1861–1873. https://doi.org/10.1021/acs.jnatprod.9b00102 (2019).
20. Sumkhemthong, S. et al. Jorunnamycin A suppresses stem-like phenotypes and sensitizes cisplatin-induced apoptosis in cancer stem-like cell-enriched spheroids of human lung cancer cells. *Mar. Drugs.* **19**, 261. https://doi.org/10.3390/md19050261 (2021).
21. Iksen, I. et al. Preclinical characterization of 22-(4′-Pyridinecarbonyl) Jorunnamycin A against lung cancer cell invasion and angiogenesis via AKT/MTOR signaling. *ACS Pharmacol. Transl Sci.* **6**, 1143–1154. https://doi.org/10.1021/acsptsci.3c00046 (2023).
22. Lee, S. Y. et al. In vitro three-dimensional (3D) cell culture tools for spheroid and organoid models. *SLAS Discov.* **28**, 119–137. https://doi.org/10.1016/j.slasd.2023.03.006 (2023).
23. Lentsch, E. et al. CRISPR/Cas9-mediated knock-out of $Kras^{G12D}$ mutated pancreatic cancer cell lines. *Int. J. Mol. Sci.* **20**, 5706. https://doi.org/10.3390/ijms20225706 (2019).
24. Cunningham, R. Subtype specific metabolic vulnerabilities in pancreatic cancer. *PhD diss. University of Glasgow*. (2020). Available from: https://eleanor.lib.gla.ac.uk/record=b3754673
25. Rückert, F. et al. Establishment and characterization of six primary pancreatic cancer cell lines. *Austin J. Cancer Clin. Res.* **2**, 1055 (2015).
26. Deer, E. L. et al. Phenotype and genotype of pancreatic cancer cell lines. *Pancreas* **39**, 425–435. https://doi.org/10.1097/MPA.0b013e3181c15963 (2010).
27. Boj, S. F. et al. Organoid models of human and mouse ductal pancreatic cancer. *Cell* **160**, 324–338. https://doi.org/10.1016/j.cell.2014.12.021 (2015).
28. Malyutina, A. et al. Drug combination sensitivity scoring facilitates the discovery of synergistic and efficacious drug combinations in cancer. *PLoS Comput. Biol.* **15**, e1006752. https://doi.org/10.1371/journal.pcbi.1006752 (2019).
29. Di Veroli, G. Y. et al. Combenefit: an interactive platform for the analysis and visualization of drug combinations. *Bioinformatics* **32**, 2866–2868. https://doi.org/10.1093/bioinformatics/btw230 (2016).
30. Cragg, G. M. & Pezzuto, J. M. Natural products as a vital source for the discovery of cancer chemotherapeutic and chemopreventive agents. *Med. Princ Pract.* **25**, 41–59. https://doi.org/10.1159/000443404 (2016).
31. Santo, V. E. et al. Drug screening in 3D in vitro tumor models: overcoming current pitfalls of efficacy read-outs. *Biotechnol. J.* **12**, 1600505. https://doi.org/10.1002/biot.201600505 (2017).
32. Shelper, T. B., Lovitt, C. J. & Avery, V. M. Assessing drug efficacy in a miniaturized pancreatic cancer in vitro 3D cell culture model. *ASSAY. Drug Dev. Technol.* **14**, 367–380. https://doi.org/10.1089/adt.2016.737 (2016).
33. Hunter, J. C. et al. Biochemical and structural analysis of common cancer-associated KRAS mutations. *Mol. Cancer Res.* **13**, 1325–1335. https://doi.org/10.1158/1541-7786.MCR-15-0203 (2015).
34. Ihle, N. T. et al. Effect of *KRAS* oncogene substitutions on protein behavior: implications for signaling and clinical outcome. *J. Natl. Cancer Inst.* **104**, 228–239. https://doi.org/10.1093/jnci/djr523 (2012).
35. Yang, Y. et al. KRAS mutations in solid tumors: characteristics, current therapeutic strategy, and potential treatment exploration. *J. Clin. Med.* **12**, 709. https://doi.org/10.3390/jcm12020709 (2023).
36. Mao, Z. et al. KRAS(G12D) can be targeted by potent inhibitors via formation of salt Bridge. *Cell. Discov.* **8**, 5. https://doi.org/10.1038/s41421-021-00368-w (2022).
37. Fell, J. B. et al. Identification of the clinical development candidate MRTX849, a covalent $KRAS^{G12C}$ inhibitor for the treatment of cancer. *J. Med. Chem.* **63**, 6679–6693. https://doi.org/10.1021/acs.jmedchem.9b02052 (2020).
38. Yang, A., Li, M. & Fang, M. The research progress of direct *KRAS* G12C mutation inhibitors. *Pathol. Oncol. Res.* **27**, 631095. https://doi.org/10.3389/pore.2021.631095 (2021).
39. He, Q., Liu, Z. & Wang, J. Targeting KRAS in PDAC: A new way to cure it? *Cancers* **14**, 4982. https://doi.org/10.3390/cancers14204982 (2022).
40. Gysin, S. et al. Therapeutic strategies for targeting Ras proteins. *Genes Cancer.* **2**, 359–372. https://doi.org/10.1177/1947601911412376 (2011).
41. Hall, B. E., Bar-Sagi, D. & Nassar, N. The structural basis for the transition from Ras-GTP to Ras-GDP. *Proc. Natl. Acad. Sci. USA* 99, 12138–12142. (2002). https://doi.org/10.1073/pnas.192453199
42. Patricelli, M. P. et al. Selective Inhibition of oncogenic *KRAS* output with small molecules targeting the inactive state. *Cancer Discov.* **6**, 316–329. https://doi.org/10.1158/2159-8290.CD-15-1105 (2016).
43. Pantsar, T. The current Understanding of KRAS protein structure and dynamics. *Comput. Struct. Biotechnol. J.* **18**, 189–198. https://doi.org/10.1016/j.csbj.2019.12.004 (2019).
44. Vasta, J. D. et al. KRAS is vulnerable to reversible switch-II pocket engagement in cells. *Nat. Chem. Biol.* **18**, 596–604. https://doi.org/10.1038/s41589-022-00985-w (2022).
45. Sun, J. M. et al. Prognostic and predictive value of *KRAS* mutations in advanced non-small cell lung cancer. *PLoS One.* **8**, e64816. https://doi.org/10.1371/journal.pone.0064816 (2013).
46. Bayat Mokhtari, R. et al. Combination therapy in combating cancer. *Oncotarget* **8**, 38022–38043. https://doi.org/10.18632/oncotarget.16723 (2017).

Acknowledgements
H.E.E.K. and R.S. acknowledge the financial support from the Second Century Fund (C2F) of Chulalongkorn University, Thailand. CP also extends thanks to Ronald Belford Scott for his support. We appreciate valuable reviews and comments from Robert Stöhr. CC and CP thank the Bavarian State Ministry of Science and the Arts, Germany, for their support through the Visiting Professor Program.

Author contributions
Conceptualization, C.P. and C.C.; methodology, C.P. and C.C.; formal analysis, H.E.E.K., U.S., T.R., S.C., Y.L., A.B., R.S., C.P., and C.C.; experimental measurement, H.E.E.K., U.S., T.R., S.C., Y.L., A.B., B.L., D.M., D.C., An.B., R.S.-S., R.G., C.P., and C.C.; writing-original draft preparation, H.E.E.K., U.S., T.R., S.C., A.B., R.G., R.S., C.P., and C.C.; editing, C.P., C.C.; project administration, C.P. and C.C.; funding acquisition, C.P. and C.C. All authors have read and agreed to the final version of the manuscript.

Funding
This research was funded by the Thailand Science Research and Innovation Fund Chulalongkorn University. R.S.-S. acknowledges the Alexander von Humboldt Foundation (Ref. 3.4-1159530THA-IP) for partially supporting this collaborative work. D.M. appreciates the grant support provided by the National Cancer Institute (NCI) of the National Institutes of Health (NIH) (Grant No. CA 150190). Additionally, A.B. expresses gratitude for the financial support from the German Research Foundation (Project number: 532458300).

Declarations

Ethics approval and consent to participate
The Ethics Committee of Friedrich-Alexander University Erlangen-Nürnberg (FAU), Germany, approved the use of human pancreatic tissue samples for this study (No. 16-167Bc). All procedures involving human pancreatic tissue samples were conducted in compliance with the ethical standards of the institutional research committee. According to the Ethics Committee, informed consent was not required from individual participants because the data analyzed in this study were anonymized and did not contain any personally identifiable information.

Consent for publication
Not applicable.

Competing interests
The authors declare no competing interests.

Supplementary Information
The online version contains supplementary material available at.
Additional file 1: Table S1 Culture media and their applications for specific cell types, Table S2 Cytotoxic effects of chemotherapeutic agents on *KRAS* G12D knockout cells, Table S3 Cytotoxic effects of jorunnamycin A and oxaliplatin on *KRAS* G12D knockout cells, Table S4 Inhibitory effects of jorunnamycin A and oxaliplatin on *KRAS* G12D knockout spheroids, Table S5 *KRAS* nucleotide sequences retrieved from patient-derived tumor and normal organoids, Fig. S1. Docking validation and RMSD value of the *KRAS* G12D binding site, Fig. S2. NMR chromatograms and LC-MS purity analysis of jorunnamycin A, Fig. S3. Validation of *KRAS* mutations (G12D, G12C, and G12V) and CRISPR/Cas9 knockout of *KRAS* G12D in pancreatic cancer cell lines via western blot analysis, Fig. S4. Cytotoxic profiles of jorunnamycin A in pancreatic cancer and normal cells, Fig. S5. Combination effect of jorunnamycin A and SN-38 in *KRAS* G12D pancreatic cancer cells, Fig. S6. Combination effect of jorunnamycin A and paclitaxel in *KRAS* G12D pancreatic cancer cells, Fig. S7. Combination effect of jorunnamycin A and 5-fluorouracil in *KRAS* G12D pancreatic cancer cells, Fig. S8. Combination effect of jorunnamycin A (JA) and gemcitabine (GEM) in *KRAS* G12D pancreatic cancer cells. Fig. S9. Variation in *KRAS* mutations in patient-derived organoids assessed by western blot analysis, Fig. S10. Morphological characteristics of patient-derived organoids following treatments with jorunnamycin A and oxaliplatin, and Figs. S11, S12, S13 and S14. Original protein bands visualized by western blot analysis supporting Figs. 3, 4 and 7, and 10 of this study.

Additional information
Supplementary Information The online version contains supplementary material available at https://doi.org/10.1038/s41598-025-95766-5.

Correspondence and requests for materials should be addressed to C.P. or C.C.

Reprints and permissions information is available at www.nature.com/reprints.

Publisher's note Springer Nature remains neutral with regard to jurisdictional claims in published maps and institutional affiliations.